

Operando Attenuated Total Reflectance FTIR Spectroscopy: Studies on the Different Selectivity Observed in Benzyl Alcohol Oxidation

Alberto Villa,^{*[a]} Davide Ferri,^[b] Sebastiano Campisi,^[a] Carine E. Chan-Thaw,^[a] Ye Lu,^[c] Oliver Kröcher,^[b, d] and Laura Prati^[a]

Au, Pd, and AuPd supported on TiO₂ were prepared by a sol immobilization route. Operando attenuated total reflectance (ATR) IR spectroscopy and catalytic batch reactor experiments were performed in parallel to elucidate the different catalytic performance of the catalysts in the liquid-phase oxidation of benzyl alcohol. Pd/TiO₂ exhibited a higher activity than AuPd/TiO₂ and Au/TiO₂, but the modification of Pd with Au demonstrated a significant stability enhancement. ATR-IR spectroscopy

evidenced that the presence of Au facilitates the desorption of byproducts, which thus reduces the extent of deactivation of the active sites caused by the irreversible adsorption of benzoate species. Although benzaldehyde was the main product in both catalysts, the nature of the byproducts differs. Pd/TiO₂ favored the deoxygenation of benzyl alcohol to produce toluene as the main byproduct. Conversely, AuPd/TiO₂ promoted the transformation of benzaldehyde to benzoic acid.

Introduction

The oxidation of alcohols to the corresponding carbonyl compounds catalyzed by supported noble metals has been a subject of growing interest recently.^[1–4] In the last decades, research has focused on green methods that use “clean” oxidants such as O₂ in combination with supported metal nanoparticles as the catalyst. Au and Pd have been studied extensively as active catalytic metals for alcohol oxidation; Au mainly for its good resistance to deactivation, and Pd for its high activity and selectivity to the corresponding aldehyde.^[1–4] However, both suffer from limitations. In particular, in the case of Au-catalyzed alcohol oxidation, a basic environment is needed to accelerate the rate-determining step (i.e., hydride abstraction), which thus enhances carboxylates as the main products.^[5–7] However, Pd suffers from severe deactivation phenomena.^[2]

It has been shown that alloyed Au-Pd catalysts have improved catalytic activity and selectivity to the desired product and also resistance to deactivation.^[8–11] This phenomenon has

been attributed to the presence of isolated single Pd sites formed in alloyed nanoparticles.^[8,12]

The selective oxidation of benzyl alcohol to benzaldehyde is a model reaction used widely and it is an important industrial process for benzaldehyde production as a key factor for fine chemicals production.^[1,2] The main byproduct of the oxidation of benzyl alcohol to benzaldehyde is toluene, which is reported to be formed by the disproportionation of benzyl alcohol^[13] or by the reaction of the intermediate metal hydride with the alcohol instead of O₂.^[14,15] A bimetallic AuPd catalyst has been shown to limit the formation of toluene.^[10,16,17]

Vibrational spectroscopy is ideally suited to interrogate the binding of molecular species on solid catalysts even if the solid is surrounded by a liquid environment. The reaction mechanism of the liquid-phase benzyl alcohol oxidation and the detailed observation of the evolution of adsorbed species have been studied extensively using attenuated total reflection (ATR) IR spectroscopy in both flow-through and batch-reactor cells.^[15] A commercial Pd/Al₂O₃ catalyst has been largely used for these measurements.^[18–20] Alcohol dehydrogenation to benzaldehyde is accompanied by both decarbonylation and oxidation of the benzaldehyde product to give benzoic acid. A number of adsorbed species have been detected and assigned to the different reaction paths at work during this reaction. Nowicka et al.^[21] studied benzyl alcohol oxidation on bimetallic Au-Pd nanoparticles dispersed on TiO₂, MgO, ZnO, and carbon by using an ATR-IR probe in a batch reactor to monitor the liquid phase by diffuse reflectance infrared Fourier transform spectroscopy (DRIFTS) and inelastic neutron scattering (INS). Only the oxidative dehydrogenation to benzaldehyde was observed on MgO and ZnO, whereas toluene was detected on the other supports, which confirmed the benzaldehyde/toluene selectivity issue.

[a] Dr. A. Villa, S. Campisi, Dr. C. E. Chan-Thaw, Prof. L. Prati
Department of Chemistry
Università degli Studi di Milano
via Golgi 19, 20133 Milan (Italy)
E-mail: alberto.villa@unimi.it

[b] Dr. D. Ferri, Prof. O. Kröcher
Paul Scherrer Institut
5232 Villigen PSI (Switzerland)

[c] Dr. Y. Lu
Laboratory for Solid State Chemistry and Catalysis
Empa, Swiss Federal Laboratories for Materials Science and Technology
Ueberlandstrasse 129, Dübendorf (Switzerland)

[d] Prof. O. Kröcher
Institut des Sciences et Ingénierie Chimiques
Ecole Polytechnique Fédérale de Lausanne (EPFL)
1015 Lausanne (Switzerland)

Ide et al. used ATR-IR spectroscopy to prove that the deactivation of Pt in alcohol oxidation is caused by the presence of species adsorbed strongly and not to metal reconstruction or leaching.^[22]

To clarify the origin of the catalytic activity of Pd/TiO₂ and AuPd/TiO₂ in liquid-phase benzyl alcohol oxidation, in this work we followed the reaction on the surface of the catalysts using ATR-IR spectroscopy. We correlated the batch catalytic results to the development of different surface species. Au, Pd, and AuPd nanoparticles were prepared by a sol immobilization procedure using polyvinyl alcohol (PVA) as a protective agent and they were supported on TiO₂ to ensure a substantially uniform particle size and distribution in the catalysts.^[23,24]

Results and Discussion

The Au, Pd, and AuPd catalysts were synthesized by sol immobilization using PVA as a protective agent.^[23,24] In particular, the bimetallic AuPd catalyst was prepared using a two-step procedure that has been demonstrated to produce alloyed AuPd NPs of a single composition and high dispersion if supported on activated carbon.^[8]

Catalyst characterization

The average diameter of TiO₂-supported Au, Pd, and AuPd nanoparticles was determined by scanning transmission electron microscopy (STEM; Table 1). Au and Pd nanoparticles showed a similar particle diameter (3.7 and 3.5 nm, respectively).

STEM data indicated a slight increase of the average particle size with the addition of Pd to the Au nanoparticles (from 3.7 to 4.1 nm). A representative overview image of AuPd/TiO₂ is given in Figure 1. Energy dispersive X-ray spectroscopy (EDX) analysis of 10 nanoparticles selected randomly indicated that they all contained both Pd and Au (Figure 1 d).

The lattice spacing of a typical AuPd nanoparticle with the nominal composition 7.4:2.6 wt% between the Pd(111) plane (2.25 Å) and the Au(111) plane (2.35 Å) was ≈ 2.29 Å (Figure 1 c), which implies the presence of an alloy.^[8] The corresponding EDX spectrum (Figure 1 d) indicates a Au/Pd ratio consistent with the nominal value (Au/Pd 7.3:2.7 wt%).

Pd/TiO₂, AuPd/TiO₂, and Au/TiO₂ were characterized by CO

Table 1. Statistical median and standard deviation of the particle size analysis for the Au, Pd, and AuPd catalysts.

Catalyst	Statistical median [nm]	Standard deviation (σ)
Au/TiO ₂	3.7	0.9
Pd/TiO ₂	3.5	0.7
AuPd/TiO ₂	4.1	1.2

adsorption to obtain a description of the native surfaces and the influence of the liquid environment on the adsorption properties of the catalysts. The DRIFT spectra recorded after 30 min adsorption under a flow of CO/He on the three catalysts are shown in Figure 2.

The corresponding spectra collected during desorption (He flow) are also shown. Signals that appear below $\tilde{\nu}=2150\text{ cm}^{-1}$ can be attributed to CO adsorbed on the noble metal particles. Typically, the adsorption of CO on metallic Pd results in signals associated with CO bound linearly (CO_L) that absorbs above $\tilde{\nu}=2000\text{ cm}^{-1}$, bridged bound CO (or twofold bound, CO_B), and finally species adsorbed on hollow sites (threefold bond, CO_{B3}).^[25–27] These two latter species give rise to a number of bands that can be divided qualitatively as follows: $\tilde{\nu}=2000\text{–}1880\text{ cm}^{-1}$ for CO_B and $\tilde{\nu}=1880\text{–}1800\text{ cm}^{-1}$ for CO_{B3}.^[28–31] The assignment of each signal is complicated by the fact that CO adsorption is site dependent, that is, the adsorption of CO (CO_L, CO_B, or CO_{B3}) on facets will give rise to signals at different frequencies from CO adsorbed in the same geometry on edges, steps, or defect sites. Coordination to facets produces higher-energy signals than coordination to particles edges/

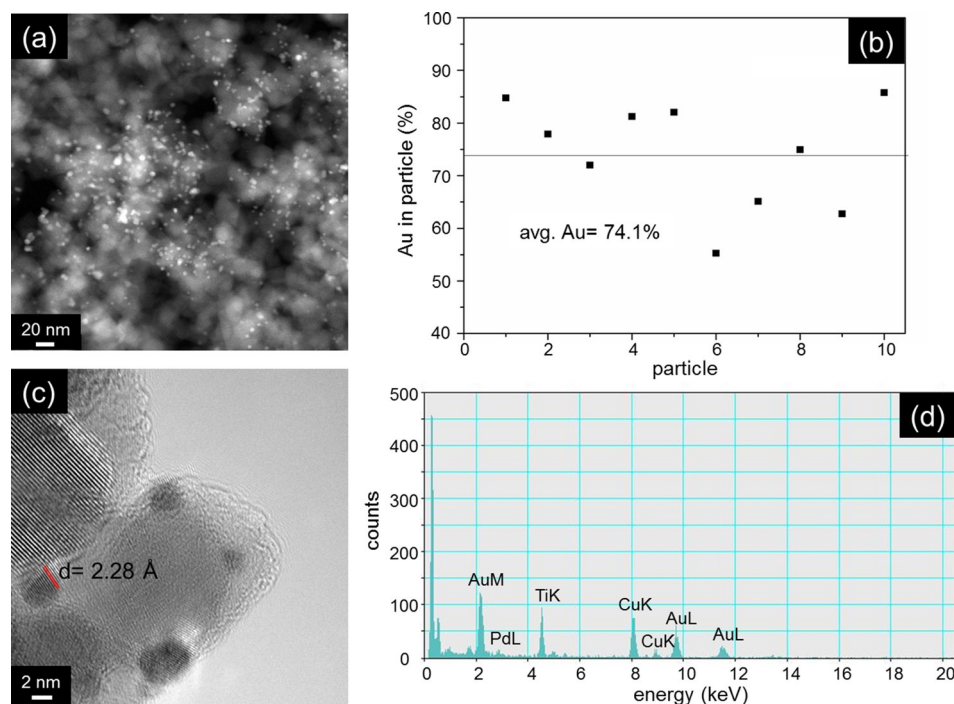


Figure 1. a) Representative STEM image, b) PdAu loading [at%] in 10 random nanoparticles of AuPd/TiO₂, c) high-resolution TEM image and d) the corresponding EDX spectrum of a AuPd particle with a Au/Pd composition of 7.4/2.6 wt%.

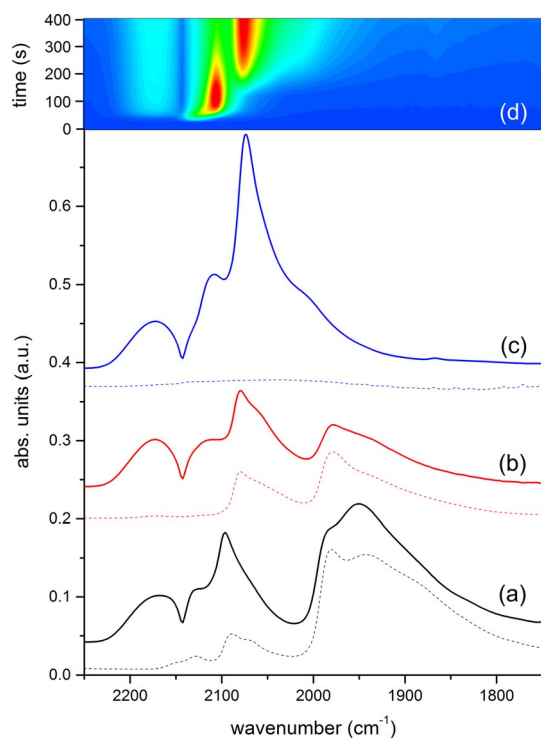


Figure 2. DRIFT spectra of adsorbed CO on a) Pd/TiO₂, b) AuPd/TiO₂, and c) Au/TiO₂. d) Color map of the time-resolved spectra recorded during CO adsorption on Au/TiO₂. Solid and dashed traces represent spectra recorded under CO/He and He flow, respectively. Spectra are offset for clarity.

steps. This can be used on a qualitative base to assess the morphology of the Pd nanoparticles using IR spectroscopy. Moreover, as the absorption coefficient of bridged species is larger than that of linear species, the CO_L/CO_B ratio represents a qualitative estimation of the size of the Pd domains.^[32]

Pd/TiO₂ exhibits signals at $\tilde{\nu}=2097$, 1981, and 1952 cm⁻¹, which are assigned to various CO species adsorbed on Pd (Figure 2a). According to the discussion above, the signals observed during CO adsorption can be attributed to CO_L and CO_B, respectively. The high energy of the CO_L signal indicates CO coordination to corner atoms, whereas the shoulder at $\tilde{\nu}\approx 2080$ cm⁻¹ is assigned to edge sites.^[25] The signals that overlap with that of gas-phase CO are most likely because of CO adsorbed on Pd²⁺ cations.^[26] This species might be present on particles that are not capped perfectly or on uncovered particles that underwent surface oxidation. According to previous reports, we assign the CO_B signal at $\tilde{\nu}=1981$ cm⁻¹ to CO coordinated to Pd(100) facets.^[26,33] The signal at $\tilde{\nu}=1952$ cm⁻¹ is thus attributed to coordination to edge/step sites. The signal is unusually intense compared to that of the high-energy CO_B species, which reveals that the Pd particles are relatively small. The spectrum measured during adsorption confirms this observation because the CO_L signal is relatively intense compared to that of CO_B.

The spectrum obtained during the subsequent He flow provides information on the species adsorbed the most strongly. The signal intensity is generally lower after desorption. Additionally, a more defined structure within the CO_L signal is ob-

tained. The shoulder at $\tilde{\nu}\approx 2070$ cm⁻¹ (edge sites) is now more pronounced. The CO_B signal loses intensity at $\tilde{\nu}=1952$ cm⁻¹ to reveal more defined signals at $\tilde{\nu}\approx 1980$ and 1900 cm⁻¹. The removal of the gas-phase signals of CO shows the signals of CO adsorbed on Pd²⁺ ($\tilde{\nu}=2145$ and 2130 cm⁻¹).

It is recognized immediately that the amount of adsorbed CO on AuPd/TiO₂ is lower than that on Pd/TiO₂ (Figure 2b). This could mean that the fraction of available metal atoms for adsorption is smaller. The spectrum measured during desorption also presents fewer signals. The absence of Pd²⁺ species ($\tilde{\nu}>2100$ cm⁻¹) suggests that all Pd present in AuPd/TiO₂ is less prone to reoxidation if exposed to air most probably because it is alloyed to Au. Importantly, we can argue that CO coordination to particle corners is suppressed by the presence of Au because the CO_L signal at $\tilde{\nu}=2097$ cm⁻¹ observed on Pd/TiO₂ is absent in this case. This allows a clear observation of the signal at $\tilde{\nu}=2079$ cm⁻¹ flanked by a shoulder on the low-energy side, which suggests adsorption on edge sites. The signal at $\tilde{\nu}=2079$ cm⁻¹ is the evident shoulder of the major CO_L signal at $\tilde{\nu}=2097$ cm⁻¹ of Pd/TiO₂. The CO_L contribution on AuPd/TiO₂ is also larger than the CO_B signal ($\tilde{\nu}=1979$ cm⁻¹). These observations indicate that small and less contiguous domains of Pd are present on the bimetallic AuPd particles in agreement with the deposition of Pd on the preformed Au nanoparticles. Although there is no evidence of CO adsorption on Au atoms, this cannot be ruled out completely given the complexity of the spectrum (Figure 2). The large difference between the spectra shown in Figure 2a and b provides a qualitative picture of the modification of Pd nanoparticles by the presence of Au, which suggests the formation of a AuPd alloy.

The adsorption of CO on Au/TiO₂ is clearly different because of the nature of the metal (Figure 2c). Adsorption first causes a signal at $\tilde{\nu}=2128$ cm⁻¹, which redshifts initially to $\tilde{\nu}=2106$ cm⁻¹. After 3 min on stream, this signal starts to transform into a signal that grows at $\tilde{\nu}=2075$ cm⁻¹ (Figure 2d). The isosbestic point at $\tilde{\nu}=2091$ cm⁻¹ indicates that the species that provides the signal initially at high frequency transforms into the species that provides the new signal. A third signal becomes visible as a shoulder at $\tilde{\nu}\approx 2020$ cm⁻¹ as this transformation occurs. All of the signals do not resist desorption, and the spectrum measured in He flow does not exhibit any signals of adsorbed CO. The signal at $\tilde{\nu}=2106$ cm⁻¹ is typically associated with CO adsorbed in a linear geometry to deficient Au atoms in Au nanoparticles.^[34] These coordinatively unsaturated atoms provide adsorption sites for CO. The intensity of the signal at $\tilde{\nu}=2128$ cm⁻¹ increases and it redshifts, which is typical for CO adsorption on Au.^[35] The change observed on Au/TiO₂ during CO adsorption is related to the reconstruction of the Au nanoparticles under the high partial pressure used in the experiment. The signal at $\tilde{\nu}=2075$ cm⁻¹ is assigned tentatively to the formation of Au⁰ sites^[34] or to negatively charged Au carbonyl species upon species absorption.^[36] Similar to Au/SiO₂,^[36] Au^{δ-} species may arise from the interaction of adsorbed CO with functional groups present on the Au particles, which are the O–H and C=O groups of the PVA capping agent in this case.

Catalytic activity in a batch reactor

The catalytic activity in the liquid-phase oxidation of benzyl alcohol was tested in a glass batch reactor using cyclohexane as the solvent. Under these reaction conditions, Au/TiO₂ was not very active (14 mol mol_{metal}⁻¹ h⁻¹; Table 2) and reached a conversion of only 12% after 8 h (Figure 3 a). This behavior confirmed previous results.^[5–7] Conversely, Pd/TiO₂ exhibited a good activity (532 mol mol_{metal}⁻¹ h⁻¹) and attained 89% conversion after 8 h (Figure 3 a).

The AuPd system showed a lower initial activity (124 mol mol_{metal}⁻¹ h⁻¹; Table 2) than the Pd system. However, after an in-

Table 2. Comparison of TiO₂-supported catalysts activities in benzyl alcohol oxidation.

Catalyst ^[a]	Activity ^[b]	Selectivity [%] ^[c]			
		Toluene	Benzaldehyde	Benzoic acid	Benzyl benzoate
Au/TiO ₂	14	–	80 ^[d]	14 ^[d]	3 ^[d]
Pd/TiO ₂	532	10	84	1	3
AuPd/TiO ₂	124	1	88	8	2

[a] Reaction conditions: alcohol/metal = 500:1 mol mol⁻¹, 60 °C, pO₂ = 2 bar, 1250 rpm. [b] Mol of reactant converted per hour per mol of metal calculated after 15 min of reaction. [c] Selectivity at 90% conversion. [d] Selectivity at 10% conversion.

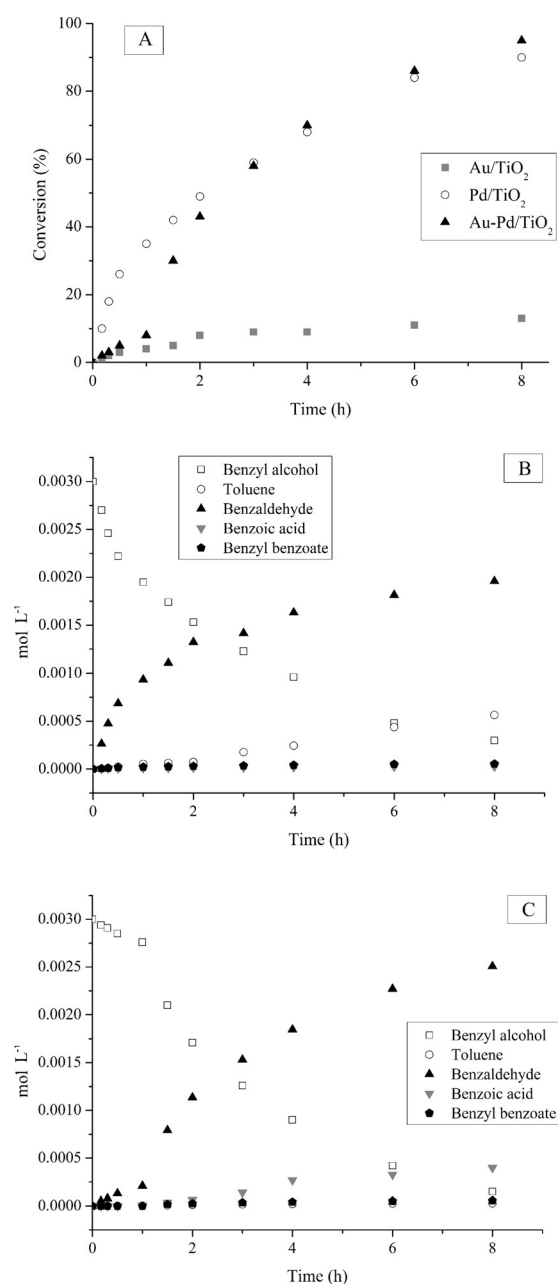


Figure 3. Reaction profiles of a) TiO₂-supported catalysts during benzyl alcohol oxidation, and the product distribution on b) Pd/TiO₂ and c) AuPd/TiO₂.

duction period, AuPd/TiO₂ (Figure 3 a) was as active as Pd/TiO₂ after 1.5 h.

If the removal of the PVA layer was involved in the origin of the induction time of AuPd/TiO₂, the same effect should have also been present in the case of Pd/TiO₂^[37] under the assumption that PVA interacts equally with the two metals. Therefore, the effect could also be because of the different nature of the active site in the bimetallic system with respect to that in the monometallic system.

With regard to the selectivity, benzaldehyde was the main product over all the catalysts (80–88% selectivity). However, the distribution of byproducts was different as can be seen from the selectivity data in Table 2 and from the evolution of the products during the reaction (Figure 3 b and c). Monometallic Pd promoted the formation of toluene (10% selectivity), the formation rate of which is linear with conversion (Figure 3 b). Conversely, in agreement with earlier results,^[10,16,17] the AuPd system did not produce toluene and promoted the consecutive transformation of benzaldehyde to benzoic acid (Table 2 and Figure 3 c) similar to the monometallic Au catalyst (Table 2).

Recycling experiments performed on the most active catalysts (Pd/TiO₂ and AuPd/TiO₂) by filtering the catalyst and adding a fresh solution of benzyl alcohol revealed the better recycling performance of AuPd/TiO₂ than Pd/TiO₂ (Figure 4), the activity of which declined very rapidly after the second run. The positive effect of bimetallic AuPd catalysts was also observed for catalysts supported on activated carbon.^[10] Inductively coupled plasma (ICP) analysis of the collected solution after six runs showed a loss of <1 wt% metal in both cases. Moreover, TEM images did not show any clear changes in the morphology of the Pd and AuPd catalysts, which had a similar particle size to the fresh materials (Table 1). Therefore, to understand the different catalytic performances, the possible role of the adsorbed species on the catalyst surface was investigated.

Operando ATR-IR spectroscopy

The evolution of surface species was monitored during the oxidation of benzyl alcohol using ATR-IR spectroscopy on particulate films deposited on an internal reflection element (IRE) mounted in a batch-reactor cell. The film was in contact with a cyclohexane solution of benzyl alcohol. As a result of the cell design, the ATR-IR spectroscopy measurements were performed at reflux (time of reaction 1 h) with oxygen bubbling

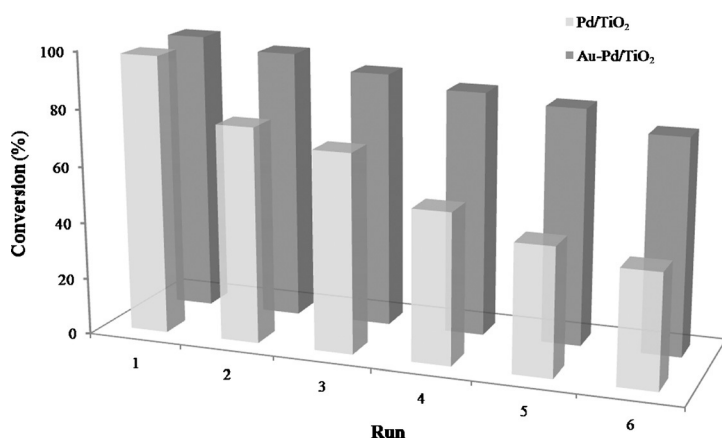


Figure 4. Stability tests performed using Pd/TiO₂ and AuPd/TiO₂.

instead of pressurizing the catalyst suspension as in the batch reactor study. This should be considered if the two sets of data are compared directly.

The ATR-IR spectra (Figure 5) obtained for the three samples are very similar and only intensity changes are observed. A sharp signal at $\tilde{\nu}=1712\text{ cm}^{-1}$ represents the benzaldehyde product dissolved in cyclohexane. The increase in the intensity of the signal is thus related to the progress of the catalytic reaction, which can be monitored by the detection of the adsorbed species. From the intensity of this signal, the order of

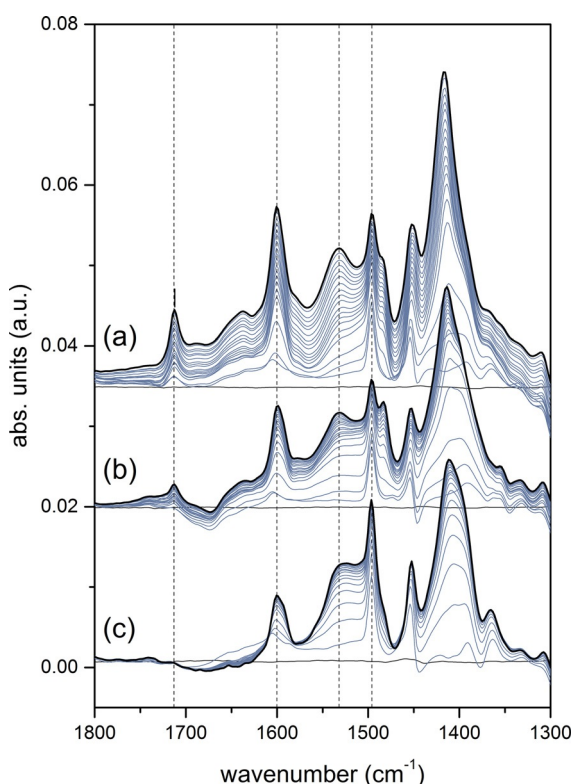


Figure 5. ATR-IR spectra recorded during benzyl alcohol oxidation on a) Pd/TiO₂, b) AuPd/TiO₂, and c) Au/TiO₂. Spectra are offset for clarity. Vertical dashed lines indicate selected signals the kinetics of which is reported in Figure 7.

the catalytic activity is Pd > AuPd > Au. The signals that develop at the early stages of the measurements at $\tilde{\nu}=1497\text{ cm}^{-1}$ and $\approx 1397\text{ cm}^{-1}$ are characteristic of benzyl alcohol, most likely dissolved in cyclohexane. The signals observed at $\tilde{\nu}=1600$ ($\nu_{\text{C}=\text{C}}$), 1531 (ν_{COOas}), 1483 ($\nu_{\text{C}=\text{C}}$), 1452 ($\nu_{\text{C}=\text{C}}$), and 1417 cm^{-1} (ν_{COOs}) belong to benzoate species, the product of benzaldehyde oxidation, which appeared to be coordinated predominantly to TiO₂.^[15] This assignment is supported by the spectra obtained upon the contact of a benzoic acid solution with TiO₂ and the corresponding metal-based catalysts (Figure 6).

The signals exhibit shoulders that likely suggest different adsorption geometries. The least pronounced signals are observed on Au/TiO₂ and the

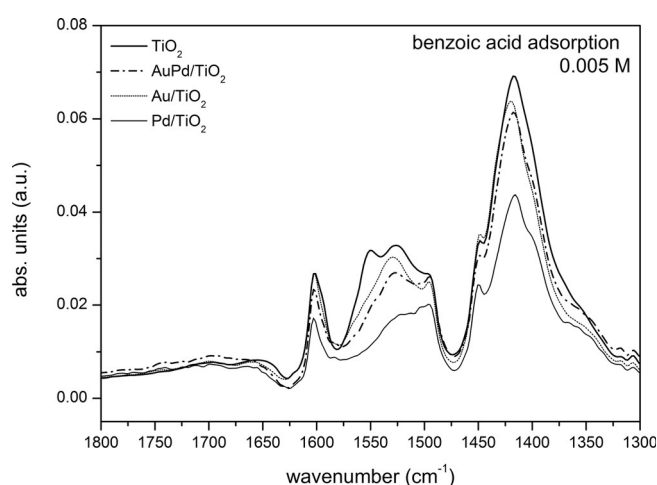


Figure 6. ATR-IR spectra recorded for benzoic acid (0.005 M solution in cyclohexane) adsorption on TiO₂, Pd/TiO₂, AuPd/TiO₂, and Au/TiO₂.

order of intensity is Pd > AuPd > Au, which is in agreement with the activity order observed in the glass reactor. This probably indicates that benzaldehyde is oxidized effectively to benzoic acid: the more benzaldehyde is produced, the more it is oxidized. Therefore, the most active Pd/TiO₂ catalyst exhibits the most intense benzoate signals. The temporal behavior of selected signals representative of dissolved benzaldehyde ($\tilde{\nu}=1712\text{ cm}^{-1}$), adsorbed benzoates ($\tilde{\nu}=1600$ and 1531 cm^{-1}), and dissolved benzyl alcohol ($\tilde{\nu}=1496\text{ cm}^{-1}$) are shown in Figure 7, which demonstrates that the rate of accumulation of adsorbed benzoate species on the three catalysts is different. Although signals grow almost linearly with time on Pd/TiO₂, they level off after a rapid initial growth on AuPd/TiO₂ and Au/TiO₂. A closer look at the spectra (Figure 6) reveals that in addition to the continuous growth of the benzoate signals on Pd/TiO₂ compared to that on AuPd/TiO₂ and Au/TiO₂, the ratio between the intensities of the signals at $\tilde{\nu}=1600$ and 1531 cm^{-1} is not equal in the three cases. This observation excludes that the signals originate only from the adsorption of benzoate species on the support. The ratio of the intensities of the bands at $\tilde{\nu}=1600$ and 1531 cm^{-1} (I_{1600}/I_{1531}) increases in the

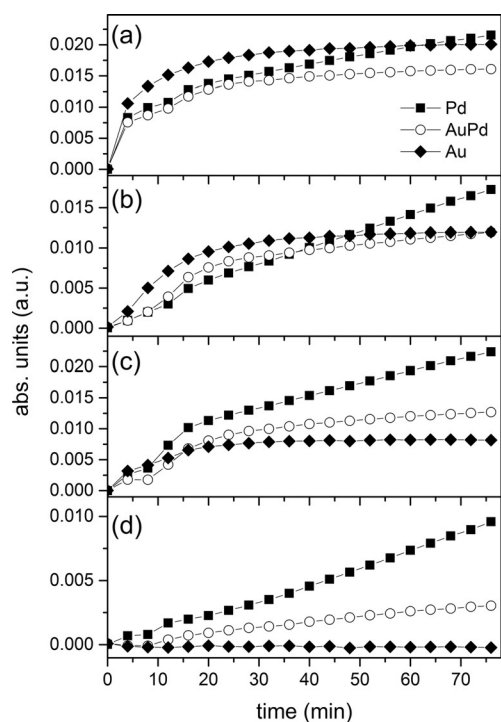


Figure 7. Time response of selected ATR-IR signals observed during benzyl alcohol oxidation on Pd/TiO₂, AuPd/TiO₂, and Au/TiO₂: a) $\tilde{\nu}=1496$, b) 1531, c) 1600, and d) 1712 cm⁻¹.

order Au < AuPd < Pd, whereas the signal at $\tilde{\nu}=1600$ cm⁻¹ seems to be accompanied by the signal of the symmetric stretch of the carboxylate group ($\tilde{\nu}=1417$ cm⁻¹). This observation suggests that an additional fraction of benzoate species is formed over the Pd-based catalysts, especially Pd/TiO₂, during reaction. It is plausible to attribute this species to benzoates adsorbed specifically on Pd particles rather than on TiO₂. These species cannot be observed if benzoates are formed from benzoic acid adsorption in the control experiments shown in Figure 6.

The assessment of conversions in these experiments using the IR signals is complicated by the overlap of the signals of the reactant and products (which include adsorbed species). The intensity of the signal of dissolved benzyl alcohol at $\tilde{\nu}=1496$ cm⁻¹ increases immediately after injection, faster than that of benzoate species, and reaches a constant intensity on the three catalysts. On Pd/TiO₂, this signal still tends to increase slightly. Its intensity is most likely more influenced by the still increasing neighboring signal at $\tilde{\nu}=1531$ cm⁻¹, which stabilizes after 30 min on Au/TiO₂ and AuPd/TiO₂.

Despite the experimental differences, the different rates of benzoate formation on Au/TiO₂ and AuPd/TiO₂ compared with that on Pd/TiO₂ and the observation of benzoate species adsorbed on Pd correlates with the selectivity obtained in the glass batch reactor study. The quantity of benzoic acid detected in solution increases in the order Pd < AuPd < Au (Table 2), which is opposite to the order detected by ATR-IR spectroscopy (Au < AuPd < Pd). The negligible amount of benzoic acid obtained with Pd/TiO₂ compared to that with AuPd/TiO₂ and

Au/TiO₂ agrees well with the preferential adsorption of these species on Pd. Previous experiments performed on Pd/Al₂O₃ evidenced that benzoic acid is formed in the early stage of the reaction and adsorbed strongly on the catalysts so that it remains undetectable in the effluent.^[15] In the case of AuPd/TiO₂ (Figure 3c), the benzoic acid concentration in the liquid phase increased clearly only after 2 h. This induction time followed the trend of the signal of benzoates observed at the surface of the catalyst. Benzoate species accumulate initially on the catalyst surface until the saturation of some specific sites, whereas benzoates formed successively desorbed into the solution. This behavior agrees with recent studies that showed that the formation of the AuPd bimetallic system alters the electronic structure of the metals, which potentially decreases the tendency for the formation of intermediates that are adsorbed strongly.^[38] The higher rate of desorption of the products, in particular that of benzoate species, on AuPd/TiO₂ compared with Pd/TiO₂ could be a possible explanation for the lower durability of the Pd catalyst compared with the bimetallic AuPd system. A similar trend was obtained for Pt-catalyzed alcohol oxidation.^[22]

Batch reactor experiments showed that the Pd catalyst promotes the formation of toluene (10%). In particular, close observation of the product distribution (Figure 3b) reveals that the rate of formation of toluene increases with increasing conversion, whereas the rate of formation of benzaldehyde shows the opposite trend. Pang et al. observed that toluene is formed in higher amounts by direct hydrogen abstraction at a high coverage of benzyl alcohol species.^[39] The presence of bimetallic AuPd nanoparticles limited the formation of toluene drastically, as reported in previous studies.^[10,16,17] Following the mechanism proposed by Pang et al.,^[39] the limited production of toluene on AuPd could correspond to reduced intermolecular interactions between adsorbed benzyl alcohol species on AuPd compared to Pd, which thus reduces the coverage of benzyl alcohol. Indeed, the time response of the ATR-IR spectra shown in Figure 7d shows that there is a higher amount of benzyl alcohol on the surface of Pd than on AuPd, in particular at high conversion ($\tilde{\nu}=1496$ cm⁻¹). Unfortunately, ATR-IR spectroscopy is not a suitable technique for the direct detection of toluene because of the overlap of the vibrational modes of toluene with those of benzyl alcohol, benzaldehyde, and adsorbed benzoate species and because of the low toluene concentration. Therefore, we could not assess the presence of toluene directly from the operando ATR-IR spectroscopy experiments and correlate it to the evolution of the observed species. Finally, no adsorbed CO derived from benzaldehyde decarbonylation was observed on all the samples, which reveals that this reaction is not favored on the catalysts prepared by sol immobilization in contrast to commercial Pd/Al₂O₃.^[15]

Conclusions

Monometallic Au and Pd and bimetallic AuPd nanoparticles were synthesized using a sol immobilization technique and were supported on TiO₂. Operando attenuated total reflectance (ATR) IR spectroscopy in a batch-reactor cell allowed us to gain

an insight into the catalytic performance of the catalysts in the liquid-phase oxidation of benzyl alcohol. In particular, the formation of AuPd bimetallic nanoparticles drastically limited the irreversible adsorption of products observed for Pd, which thus decreased the extent of catalyst deactivation. This technique also showed that the presence of Au facilitates the desorption of the products, especially benzoate species. All the catalysts demonstrated a good selectivity to benzaldehyde (78–83%). However, toluene was produced as the main byproduct (16%) on the monometallic Pd catalyst. The modification of Pd with Au suppressed the formation of toluene by reducing the amount of benzyl alcohol on the surface. Conversely, it promoted the transformation of benzaldehyde to benzoic acid.

Experimental Section

Catalyst preparation

Monometallic catalysts

Au catalyst preparation: Solid $\text{NaAuCl}_4 \cdot 2\text{H}_2\text{O}$ (Aldrich, 99.99% purity; 0.043 mmol) and PVA solution ($MW_{\text{PVA}} = 13\,000\text{--}23\,000$, 87–89% hydrolyzed, Aldrich; 1% w/w; Au/PVA 1:0.5, w/w) were added to H_2O (100 mL). After 3 min, NaBH_4 (Fluka, >96%; Au/ NaBH_4 1:4 mol/mol) solution was added to the solution with vigorous magnetic stirring. A ruby-red Au^0 sol was formed immediately. The UV/Vis spectrum of the Au sol was recorded to check the complete reduction of AuCl_4^- and the formation of the plasmon peak of Au^0 nanoparticles. Within a few minutes from its generation, the colloid (acidified at pH 2 by sulfuric acid) was immobilized by adding the support (TiO_2 , Degussa P25, $49\text{ m}^2\text{g}^{-1}$, 80% anatase) under vigorous stirring. The amount of support was calculated to obtain a final metal loading of 1 wt%. The catalysts were filtered, washed several times, dried at $80\text{ }^\circ\text{C}$ for 4 h.

Pd catalyst preparation: Solid Na_2PdCl_4 (Aldrich, 99.99% purity; Pd 0.043 mol) and PVA solution (1% w/w, Pd/PVA 1:0.5 w/w) were added to H_2O (100 mL). After 3 min, NaBH_4 (Pd/ $\text{NaBH}_4 = 1:8$ mol/mol) solution was added to the yellow-brown solution with vigorous magnetic stirring. The brown Pd^0 sol was formed immediately. A UV/Vis spectrum of the Pd sol was recorded to check the complete reduction of PdCl_4^{2-} . Within few minutes from its generation, the colloid (acidified at pH 2 by sulfuric acid) was immobilized by adding the support under vigorous stirring. The amount of support was calculated to obtain a final metal loading of 1 wt%. The catalysts were filtered, washed several times, and dried at $80\text{ }^\circ\text{C}$ for 4 h.

Bimetallic catalysts

Bimetallic catalysts have been prepared following a procedure reported previously.^[8] After the preparation of 0.73 wt% Au/ TiO_2 according to the procedure reported above, the material was dispersed in water (100 mL), and Na_2PdCl_4 (Pd 0.025 mol) and PVA solutions (1% w/w, Pd/PVA 1:0.5 w/w) were added. H_2 was bubbled (50 mL min^{-1}) under atmospheric pressure at RT. After 2 h, the slurry was filtered, and the catalyst was washed thoroughly with distilled water.

ICP analysis was performed on the filtrate to verify the quantitative metal loading on the support. The final total metal loading was 1 wt% in all cases. For the bimetallic catalyst, the Au/Pd ratio was 7.3:2.7 wt% (6:4 mol/mol).

Catalytic test in a batch reactor

The reactions were performed in a thermostatted glass reactor (30 mL) provided with an electronically controlled magnetic stirrer connected to a large reservoir (5000 mL) that contained oxygen at 2 bar (SIAD, 99.99%). The oxygen uptake was followed by a mass flow controller connected to a PC through an A/D board, which plotted a flow–time diagram. The oxidation experiments were performed in the presence of cyclohexane (Sigma–Aldrich, puriss. p. a. ACS reagent, $\geq 99.5\%$, GC) as the solvent and 0.3 M benzyl alcohol (Sigma–Aldrich, puriss., meets analytical specification of Ph. Eur., BP, NF, 99–100.5%, GC; substrate/metal = 500 mol/mol, $60\text{ }^\circ\text{C}$, $p\text{O}_2 = 2$ bar). The periodic removal of samples from the reactor was performed. Mass recoveries were always $(98 \pm 3)\%$ with this procedure. For the identification and analysis of the products, a GC HP 7820 A gas chromatograph equipped with a capillary column (HP-5, $30\text{ m} \times 0.32\text{ mm}$, $0.25\text{ }\mu\text{m}$ film, Agilent Technologies) and thermal conductivity detector (TCD) was used. Quantification of the reaction products was performed by the external calibration method.

Catalyst characterization

The morphology of the catalysts was observed by using a Jeol 2200FS transmission electron microscope equipped with a 200 kV field-emission gun and a high-angle annular dark field detector in STEM mode. The local composition was determined by EDX. The samples were prepared by evaporation of an alcohol suspension on a copper grid coated with a holey carbon film. The noble metal particle size distribution was obtained by measuring particles by using the software ImageJ.

DRIFT spectra were collected by using a Vertex 70 (Bruker Optics) spectrometer equipped with a liquid-nitrogen-cooled mercury cadmium telluride (MCT) detector and a commercial mirror unit (Praying Mantis, Harrick). CO adsorption from the gas phase was followed at RT on as-received catalysts by admitting 50 mL min^{-1} 5 vol% CO/He after dehydration for 1 h at $120\text{ }^\circ\text{C}$ in He and by accumulating spectra (first 100 scans, 14 s/spectrum; then 200 scans, ca. 180 s/spectrum; 4 cm^{-1} resolution) over 30 min. Adsorbed CO was then replaced by He to follow desorption under otherwise identical conditions. The powder samples (≈ 70 mg) were used without further dilution. Spectra were normalized against a background spectrum recorded in He flow before the admittance of CO. All spectra are presented in absorbance units and were corrected for contribution of atmospheric CO_2 and water if needed.

A homemade batch-reactor cell was used to monitor alcohol oxidation both on the surface of the catalyst and in solution using the ATR mode.^[18] The cell is a modification of that described in Ref. [40]. Stirring was provided by using a conventional laboratory magnetic stirrer integrated in the base plate of the cell. The top of the cell was fitted with a stainless-steel cover with a circular aperture that allowed the insertion of a glass condenser (conical tapered ground joint, 19/26) for experiments under reflux. The ZnSe IRE (30° , $50\text{ mm} \times 20\text{ mm} \times 2\text{ mm}$; Crystran Ltd.) was coated with a powder film obtained by the evaporation of a catalyst suspension ($15\text{ mg}/2\text{ mL}$ suspension) and was placed on the horizontal heatable base of the cell. After mounting the cell body and adding 20 mL of cyclohexane solvent, the temperature was increased to $60\text{ }^\circ\text{C}$, and the system was left to equilibrate for ≈ 2 h under bubbling N_2 at reflux and stirring. Before the injection of benzyl alcohol ($190\text{ }\mu\text{L}$), a background IR spectrum of the catalyst was recorded at $60\text{ }^\circ\text{C}$ in cyclohexane. Then a series of consecutive ATR-IR spectra (200 scans, $\approx 4\text{ min/spectrum}$, 4 cm^{-1} resolution) were collected to

follow the reaction. After ≈ 5 min from the injection of benzyl alcohol, N_2 was replaced by O_2 , and the system was allowed to react for ≈ 1 h. The metal content of the catalyst and the metal leaching during the experiments were checked by the ICP analysis of the filtrate by using a JobinYvon JY24.

Keywords: IR spectroscopy · gold · nanoparticles · oxidation · palladium

- [1] M. Besson, P. Gallezot, *Catal. Today* **2000**, *57*, 127–141.
- [2] T. Mallat, A. Baiker, *Chem. Rev.* **2004**, *104*, 3037–3058.
- [3] N. Dimitratos, J. A. Lopez-Sanchez, G. J. Hutchings, *Chem. Sci.* **2012**, *3*, 20–44.
- [4] S. E. Davis, M. S. Ide, R. J. Davis, *Green Chem.* **2013**, *15*, 17–45.
- [5] S. Carrettin, P. McMorn, P. Johnston, K. Griffin, C. J. Kiely, G. J. Hutchings, *Phys. Chem. Chem. Phys.* **2003**, *5*, 1329–1336.
- [6] F. Porta, L. Prati, *J. Catal.* **2004**, *224*, 397–403.
- [7] S. Demirel-Gülen, M. Lucas, P. Claus, *Catal. Today* **2005**, *102–103*, 166–172.
- [8] D. Wang, A. Villa, F. Porta, D. Su, L. Prati, *Chem. Commun.* **2006**, 1956–1958.
- [9] D. I. Enache, J. K. Edwards, P. Landon, B. Solsona-Espriu, A. F. Carley, A. A. Herzing, M. Watanabe, C. J. Kiely, D. W. Knight, G. J. Hutchings, *Science* **2006**, *311*, 362–365.
- [10] A. Villa, D. Wang, N. Dimitratos, D. Su, V. Trevisan, L. Prati, *Catal. Today* **2010**, *150*, 8–15.
- [11] W. Hou, N. A. Dehm, R. W. J. Scott, *J. Catal.* **2008**, *253*, 22–27.
- [12] M. Chen, D. Kumar, C. W. Yi, D. W. Goodman, *Science* **2005**, *310*, 291–293.
- [13] M. Sankar, E. Nowicka, P. J. Miedziak, G. L. Brett, R. L. Jenkins, N. Dimitratos, S. H. Taylor, D. W. Knight, D. Bethell, G. J. Hutchings, *Faraday Discuss.* **2010**, *145*, 341–356.
- [14] A. Savara, C. E. Chan-Thaw, I. Rossetti, A. Villa, L. Prati, *ChemCatChem* **2014**, *6*, 3464–3473.
- [15] C. Keresszegi, D. Ferri, T. Mallat, A. Baiker, *J. Phys. Chem. B* **2005**, *109*, 958–967.
- [16] A. Villa, D. Wang, P. Spontoni, R. Arrigo, D. Su, L. Prati, *Catal. Today* **2010**, *157*, 89–93.
- [17] Q. He, P. J. Miedziak, L. Kesavan, N. Dimitratos, M. Sankar, J. A. Lopez-Sanchez, M. M. Forde, J. K. Edwards, D. W. Knight, S. H. Taylor, C. J. Kiely, G. J. Hutchings, *Faraday Discuss.* **2013**, *162*, 365–378.
- [18] D. Ferri, A. Baiker, *Top. Catal.* **2009**, *52*, 1323–1333.
- [19] C. Mondelli, J. Grunwaldt, D. Ferri, A. Baiker, *Phys. Chem. Chem. Phys.* **2010**, *12*, 5307–5316.
- [20] C. Keresszegi, D. Ferri, T. Mallat, A. Baiker, *J. Catal.* **2005**, *234*, 64–75.
- [21] E. Nowicka, J. P. Hofmann, S. F. Parker, M. Sankar, G. M. Lari, S. A. Kondrat, D. W. Knight, D. Bethell, B. M. Weckhuysen, G. J. Hutchings, *Phys. Chem. Chem. Phys.* **2013**, *15*, 12147–12155.
- [22] M. S. Ide, D. D. Falcone, R. J. Davis, *J. Catal.* **2014**, *311*, 295–305.
- [23] L. Prati, G. Martra, *Gold Bull.* **1999**, *32*, 96–101.
- [24] L. Prati, A. Villa, *Acc. Chem. Res.* **2014**, *47*, 855–863.
- [25] A. R. Denton, N. W. Ashcroft, *Phys. Rev. A* **1991**, *43*, 3161–3164.
- [26] T. Lear, R. Marshall, J. A. Lopez-Sanchez, S. D. Jackson, T. M. Klapötke, M. Bäumer, G. Rupprechter, H. J. Freund, D. Lennon, *J. Chem. Phys.* **2005**, *123*, 174706–174713.
- [27] D. Tessier, A. Rakai, F. Bozon-Verduraz, *J. Chem. Soc. Faraday Trans.* **1992**, *88*, 741–749.
- [28] N. Sheppard, C. De La Cruz, *Catal. Today* **2001**, *70*, 3–13.
- [29] N. Sheppard, T. T. Nguyen in *Advanced Infrared Raman Spectroscopy, Vol. 5* (Eds.: R. J. H. Clark, R. E. Hester), Heyden, London, **1978**, pp. 67–148.
- [30] C. De La Cruz, N. Sheppard, *J. Mol. Struct.* **1990**, *224*, 141–161.
- [31] E. Ozensoy, D. W. Goodman, *Phys. Chem. Chem. Phys.* **2004**, *6*, 3765–3778.
- [32] M. A. Vannice, S. Y. Wang, *J. Phys. Chem.* **1981**, *85*, 2543–2546.
- [33] F. Di Gregorio, L. Bisson, T. Armaroli, C. Verdon, L. Lemaitre, C. Thoma-zeau, *Appl. Catal. A* **2009**, *352*, 50–60.
- [34] E. Roze, P. Gravejat, E. Quinet, J. L. Rousset, D. Bianchi, *J. Phys. Chem. C* **2009**, *113*, 1037–1045.
- [35] F. Boccuzzi, A. Chiorino, M. Manzoli, P. Lu, T. Akita, S. Ichikawa, M. Haruta, *J. Catal.* **2001**, *202*, 256–267.
- [36] K. Chakarova, M. Mihaylov, S. Ivanova, M. A. Centeno, K. Hadjiivanov, *J. Phys. Chem. C* **2011**, *115*, 21273–21282.
- [37] A. Villa, D. Wang, G. M. Veith, F. Vindigni, L. Prati, *Catal. Sci. Technol.* **2013**, *3*, 3036–3041.
- [38] M. B. Griffin, A. A. Rodriguez, M. M. Montemore, J. R. Monnier, C. T. Williams, J. W. Medlin, *J. Catal.* **2013**, *307*, 111–120.
- [39] S. H. Pang, A. M. Roman, J. W. Medlin, *J. Phys. Chem. C* **2012**, *116*, 13654–13660.
- [40] B. Panella, A. Vargas, D. Ferri, A. Baiker, *Chem. Mater.* **2009**, *21*, 4316–4322.

Received: April 20, 2015

Published online on July 16, 2015